COVID-19-Induced Changes in the Fibrin Network of Pulmonary and Renal Microthrombi

Manuel Meneses-Flores[1, 2], Jose S. Lopez-Gonzalez[1], Eduardo Becerril-Vargas[3], Saray Santos-Torres[2], Francina Bolaños-Morales[4], Dolores Aguilar-Cazares[1], Cesar Luna-Rivero[2,*]

[1]Department of Chronic-Degenerative Diseases. Instituto Nacional de Enfermedades Respiratorias Ismael Cosío Villegas. Mexico City, Mexico.

[2]Department of Pathological Anatomy. Instituto Nacional de Enfermedades Respiratorias Ismael Cosío Villegas. Mexico City, Mexico.

[3]Clinical Microbiology Lab. Instituto Nacional de Enfermedades Respiratorias Ismael Cosío Villegas. Mexico City, Mexico.

[4]Department of Thoracic Surgery. Instituto Nacional de Enfermedades Respiratorias Ismael Cosío Villegas. Mexico City, Mexico.

Research Article

Open Access &

Peer-Reviewed Article

DOI: 10.14302/issn.2692-1537.ijcv-24-5218

Running title:

Fibrin Network Alterations in COVID-19 Microthrombi

Corresponding author:

Cesar Luna-Rivero, Department of Pathological Anatomy Instituto Nacional de Enfermedades Respiratorias Ismael Cosío Villegas. Tlalpan 4502. Col. Sección XVI. CP 14080. Mexico City, Mexico

Keywords:

SARS-CoV-2, Autopsy, Lung , Kidney, Microthombi, Fibrin Network

Received: July 31, 2024

Accepted: August 31, 2024

Published: September 25, 2024

Citation:

Manuel Meneses-Flores, Jose S. Lopez-Gonzalez, Eduardo Becerril-Vargas, Saray Santos-Torres, Francina Bolaños-Morales et al. (2024) COVID-19 -Induced Changes in the Fibrin Network of Pulmonary and Renal Microthrombi. International Journal of Coronaviruses - 5(1):18-29. https://doi.org/10.14302/issn.2692-1537.ijcv-24-5218

Abstract

Background

Severe acute respiratory syndrome coronavirus 2 (SARS-CoV-2) infection often causes coagulation disorders that affect highly vascularized organs, such as the lungs and kidneys.

Objective

The objective of this study was to report the histopathological findings of variations in the fibrin pattern of pulmonary and renal microthrombi in patients who died from SARS-CoV-2 infection.

Methods

Minimally invasive autopsies were performed on 40 patients to collect lung (n=40) and kidney (n=16) tissue samples. Histochemical and immunohistochemical staining techniques were used for histopathological analyses. Premortem laboratory data were obtained from the patients' electronic medical records.

Results

The lung tissue showed a patchy pattern, characterized by areas of both minimal and severe damage. The most significant histopathological finding was the detection of thrombi with fibrin structures organized into discrete star-shaped units, which were more frequently observed in areas with severe lung injury than in those with minimal lung injury ($p = 0.012$). Star-shaped fibrin structures were also observed in the renal glomerular capillaries. Immunohistochemical staining revealed the presence of platelets and the procoagulant proteins von Willebrand factor (VWF) and Factor VIII within the star-shaped fibrin thrombi. Patients with

star-shaped fibrin thrombi had higher levels of the systemic inflammatory indicators C-reactive protein (CRP) and neutrophil-to-lymphocyte ratio (NLR).

Conclusion

Our observations suggest that the inflammatory microenvironment resulting from SARS-CoV-2 infection may contribute to the formation of star-shaped fibrin units in the pulmonary and renal microthrombi.

Background

Coronavirus disease 2019 (COVID-19), caused by severe acute respiratory syndrome coronavirus 2 (SARS-CoV-2), was declared a pandemic by the World Health Organization (WHO) in March 2020. SARS-CoV-2 is closely related to SARS-CoV, the virus responsible for the outbreak of severe acute respiratory syndrome (SARS) in 2003. Both viruses infect cells through angiotensin-converting enzyme 2 (ACE2) receptors, which negatively regulate the human renin-angiotensin-aldosterone system (RAAS) and play a critical role in the control of blood pressure and blood volume. This regulation is essential for the normal functioning of various organs, including the lungs, heart, kidneys, and blood vessels. Endothelial cells are among the primary cell types that express ACE2, rendering highly vascularized organs particularly susceptible to direct SARS-CoV-2 infection.

One of the main consequences of viral infection is dysregulation of hemostasis due to the release of tissue factors caused by severe damage to vascular endothelial cells and the cytokine storm generated by the immune system in response to SARS-CoV-2 infection. This creates a hypercoagulable environment that promotes the formation of blood clots in pulmonary arterioles and alveolar capillaries. Simultaneously, fibrin clumps are deposited in the alveolar spaces, exacerbating symptoms of acute respiratory distress syndrome (ARDS).

A meta-analysis of autopsy series of COVID-19 patients revealed that the main histological damage in the lungs was diffuse alveolar damage (DAD) in different clinical phases, whereas acute tubular injury was the main finding in the kidneys. An important finding in COVID-19 autopsies is the detection of platelet-fibrin thrombi in the small pulmonary vessels. Fibrin plays a key role in thrombus formation by inducing a mesh-like structure that serves as a scaffold to reinforce the initial platelet plug formed at the injury site. Because the fibrin structure of microthrombi from COVID-19 patients has not been the subject of previous studies, the objective of this study was to report the histopathological findings of a variation in the structural pattern of fibrin in pulmonary and renal microthrombi from a set of patients who died as a result of SARS-CoV-2 infection.

Methods

Patients

All patients (n = 40) were diagnosed with SARS-CoV-2 infection as confirmed by real-time reverse transcriptase-polymerase chain reaction (RT-PCR) testing of nasopharyngeal specimens at the time of hospital admission. All patients admitted to the hospital were in critical condition and required mechanical ventilation from the first day of hospitalization. Enoxaparin-based anticoagulant therapy and antiviral therapy with tocilizumab, lopinavir, and ritonavir were administered. For bacterial infections, patients were treated with intravenous antibiotics, vancomycin, clarithromycin, and azithromycin. None of the patients had been vaccinated. Medical and laboratory records were reviewed to obtain the demographic, clinical, and laboratory data. The study protocol was carried out in

accordance with the Declaration of Helsinki and was approved by the Scientific, Ethics, and Biosafety Committees of INER (B05-24).

Autopsies, Biopsy Collection, and Tissue Processing

Postmortem biopsies were obtained from 40 individuals who died between April 15, 2020, and August 20, 2021. The autopsies were initiated between three and five hours after the subject's estimated time of death. The procedure was performed using minimally invasive techniques. Lung samples (n=40) were obtained via a unilateral thoracotomy. For the kidney samples (n=16), a Tru-Cut needle (20 G X15 cm) was used for biopsy, and the tissues were subsequently fixed in neutral-buffered formalin for 24 hours before processing. Paraffin-embedded sections (3-µm thickness) were stained with hematoxylin and eosin (H&E) to detect pathological changes. Phosphotungstic acid-hematoxylin (PTAH), a specific method for fibrin staining, was used to demonstrate the presence of fibrin in the thrombi. Immunohistochemical staining was performed using the peroxidase method with the following antibodies: anti-CD61 (2f2, Bio SB) for platelets, anti-von Willebrand Factor (VWF) (GTX26994; Genetex), and anti-factor VIII (Biocare Medical CP 039) for procoagulant proteins. Diaminobenzidine was used as a substrate for color development. Tissue sections were counterstained with Harry's hematoxylin and observed by two experienced pneumopathologists. In cases of discrepancies, the material was reviewed jointly to reach a final decision.

Microscopic images were captured using a DFC425 C color camera (Leica Microsystems Inc., Wetzlar, Germany) mounted on a Leica DMLB optical microscope and processed using the Leica Application Suite v software version 3.6.0 (Leica Microsystems Inc.).

Statistical Analysis

Quantitative variables were analyzed using one-way analysis of variance followed by Tukey's test for comparisons among three groups, and two-tailed t-tests for comparisons between two groups. Qualitative variables were analyzed using Fisher's exact test. Statistical significance was set at $p < 0.05$. Statistical analysis was performed with the package available online at https://www.socscistatistics.com/tests/.

Results

Clinical and Demographic Data

The study population comprised 40 subjects, including 8 females and 32 males, with mean ages of 62.6 ± 9.7 years and 57.9 ± 15.5 years, respectively. All the patients were infected with SARS-CoV-2. Fibrin thrombi were identified in 33 out of 40 patients (82.5%), and bacterial co-infections were detected in 33/40 (70%) of the cases (Table 1). The most frequently isolated microorganisms included *Acinetobacter baumannii, Klebsiella pneumoniae, Pseudomonas aeruginosa, Staphylococcus epidermidis and Stenotrophomonas maltophilia*.

The most common comorbidities in the population were systemic arterial hypertension, diabetes mellitus, acute kidney injury, and obesity (Table 1).

Respiratory, Coagulation, and Inflammation Parameters

In light of the study's primary objective, which was to examine the structural pattern of fibrin in thrombi, patients with thrombi were classified into two groups, designated as the "Star-shaped pattern" and the "Reticular pattern" (Table 2), based on the observed fibrin structure in their thrombi. The analysis of the PaO_2/FiO_2 ratio and oxygen saturation ($SatO_2$) revealed no significant differences

Table 1. Demographic, bacterial co-infection, and comorbidity data of 40 patients who died from COVID-19 between April 15, 2020, and August 20, 2021, at the National Institute of Respiratory Diseases. The sample was divided into three subgroups based on the fibrin pattern observed in their thrombi.

	Fibrin structure in thrombi				
	Star-shaped	RTP	Thrombi	Total	p
Patients (n)	7	26	7	40	
Age (yr)**	65.9.3 ± 13.8	57.1 ± 13.5	52.7 ± 18.1	55.5 ± 14.9	0.224
females	2	5	1	8	
males	5	21	6	32	
Fibrin thrombi + (%)	100	100	0	82.5	
Hospital stay (d)**	11.3 ± 5.8	17.1 ± 11.3	14.6 ± 4.1	15.0 ± 9.9	0.367
Co-infection (%)					
CAI	14.3	11.5	42.9	17.5	
HAI	57.1	57.7	28.6	52.5	
PWO co-infection	28.6	30.8	28.6	30	
Total	71.4	69.2	71.4	70	
Comorbidities (%)					
DM	28.6	38.5	28.6	35	
SAH	42.9	38.5	42.9	40	
AKI	14.3	30.8	28.6	27.5	
BMI**	32.9 ± 6.2	32.7 ± 8.2	27.7 ± 0.5	32.4 ± 7.6	0.251

Abbreviations
*Thrombi Non detectado; ** mean ± standard deviation; CAI - Community-acquired co-infection; HAI - Hospital-acquired co-infection; PWO co-infection - Patients without co-infection; DM - Diabetes mellitus; SAH - Systemic arterial hypertension; AKI - Acute Kidney Injury; BMI - Body Mass Index.

between the two groups (Table 2). Coagulation parameters, including prothrombin time, activated partial thromboplastin time, thrombin time, and D-dimer levels, were elevated above their respective reference values. However, no statistically significant differences were observed between the groups (Table 2). However, analysis of inflammatory indicator parameters indicated that the group of patients with thrombi exhibiting a star-shaped fibrin structure exhibited higher levels of C-reactive protein and neutrophil-to-lymphocyte ratio than the group of patients with a reticular fibrin pattern. Nevertheless, only CRP concentration exhibited a statistically significant difference (Table 2).

Histopathological Analysis

Lung

The lung tissue showed a patchy pattern, including areas with minimal and severe damage, separated by the interlobular septum. In areas exhibiting severe damage, interstitial thickening, edema, and inflammatory infiltrates, comprising neutrophils and lymphocytes, were observed. In contrast, regions

Table 2. Coagulation, inflammatory parameters, and fibrin structure patterns in thrombi from deceased COVID-19 patients between April 15, 2020, and August 20, 2021, at the National Institute of Respiratory Diseases.

Parameters	Normal Range	Fibrin Patern		P values
		Star-shaped	Reticular	
n	N/A	7	26	N/A
PT (sec)	10.2 - 13.2	16.2 ± 2.4	16.3 ± 1.9	0.929
INR	0,72 - 1,24	1.1 ± 0.2	1.1 ± 0.1	0.868
aTTP (sec)	26,5 - 32,5	54.4 ± 21.3	45.0 ± 9.8	0.093
TT (sec)	16 - 25	25.8 ± 10.9	27.75± 11.9	0.734
PCT (µg/ml)	0 - 0,5	3.2 ± 2.2	2.5 ± 4.3	0.671
D-dimer (µg/ml)	< 0.5	1.7 ± 0.7	3.3± 2.8	0.153
CRP (mg/dl)	< 1.0	28.4 ± 13.0	15.4 ± 8.0	**0.003**
NLR	0.78 – 3.53	18.7 ± 8.9	13.1 ± 6.4	0.068
PaO_2/FiO_2 (mmHg)	≥ 300	98.0 ± 25.7	135.7 ± 44.4	0.116
Sat o_2 (%)	95 -100	88.8 ± 8.0	80.4 ± 12.8	0.223

Abbreviations:
PT - Prothrombin time; INR - International normalized ratio; aPTT - Activated partial thromboplastin time; TT - Thrombin time; CRP - C-reactive protein; NLR - Neutrophil-to-lymphocyte ratio; PaO_2/FiO_2 - Ratio of arterial partial pressure of oxygen to the fraction of inspired oxygen; Sat O_2 - Oxygen saturation.

Note: p-values marked in bold are statistically significant.

exhibiting minimal damage displayed a paucity of the previously listed histopathological findings (Fig. 1A). Hyaline membranes, pneumocyte detachment, intra-alveolar fibrin deposition, and alveolar macrophages were observed in the alveolar lumen in both areas regardless of the severity of the injury (Fig. 1A and 2A). The presence of thrombi was documented in both the arterioles (29/33) and pulmonary capillaries (19/33). In general, the pulmonary thrombi showed a characteristic reticular fibrin pattern (Fig. 2C-D). However, in addition to this fibrin pattern, in 4/33 (12%) cases, the fibrin scaffold of the thrombus was observed to have a different arrangement than that of the classic reticular structure. Since we did not find any references describing this pattern, we call it "star-shaped fibrin pattern."

Thrombi with star-shaped fibrin structures were observed in the pulmonary arterioles and capillaries (Fig. 2E-F), predominantly in areas of severe lung injury (Fig. 1C-E). Intra-alveolar fibrin deposits were observed in 24 of the 33 cases, but no star-shaped structures were observed, regardless of the severity of lung injury (Fig. 2A-B). PTAH staining of the star-shaped structures demonstrated that they were composed of fibrin (Fig. 2E-F and 3A). Similarly, immunohistochemical staining with CD61 demonstrated the presence of platelet clumps (Fig. 3B), which expressed the procoagulant proteins VWF (Fig. 3C) and Factor VIII (Fig. 3D). Erythrocytes were not observed in fibrin structures.

Kidney

Histopathological examination of renal tissue revealed tubular degenerative changes and glomerular

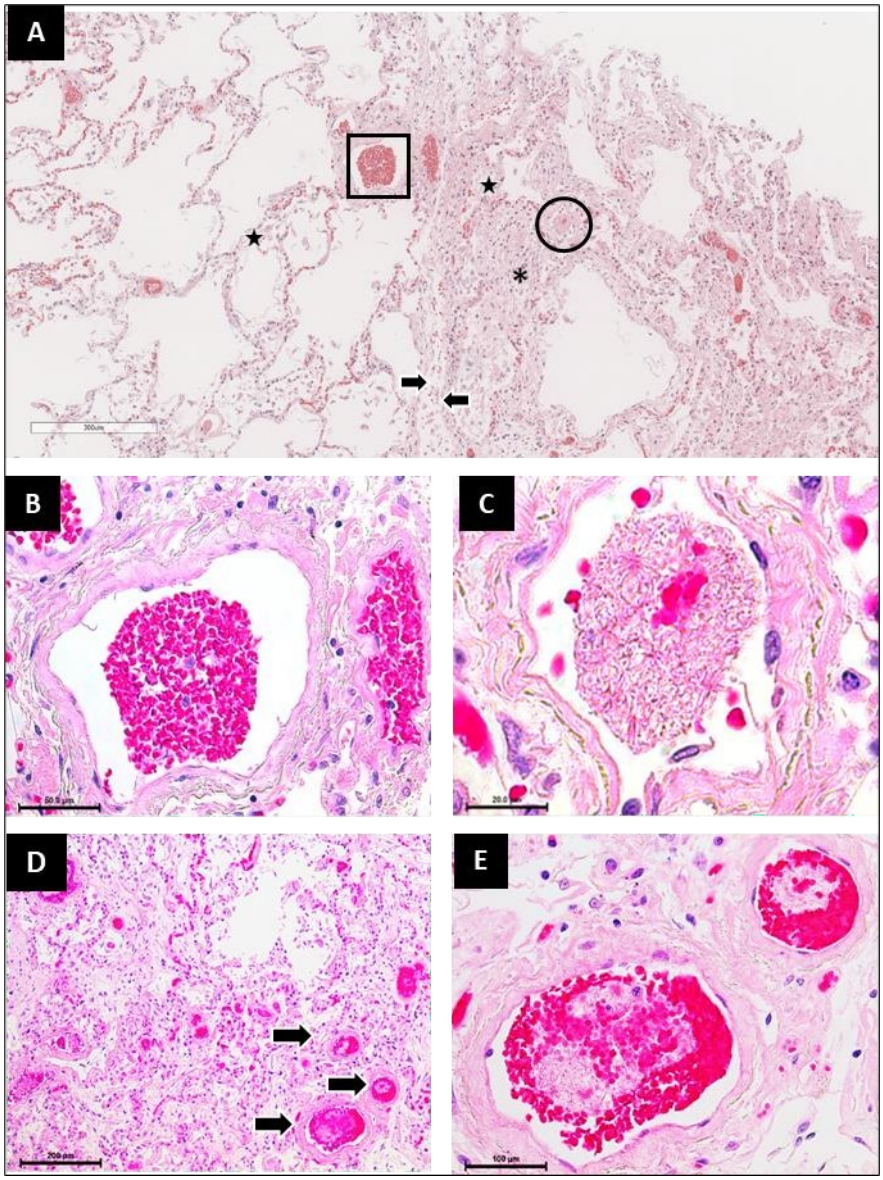

Figure 1. Fibrin thrombi in areas of minimal and severe damage in the lungs of patients who died of SARS-CoV-2 infection.

(A) Panoramic micrograph showing a patchy pattern with areas of minimal (left) and severe (right) damage, separated by the interlobular septum (arrows). The square highlights a normal blood vessel (left), while the circle highlights a blood vessel with a fibrin embolus (right). Stars indicate alveolar spaces containing alveolar macrophages and pneumocyte detachment. The asterisk indicates areas of inflammatory infiltrate and interstitial thickening. (B, C) Magnification of the blood vessels highlighted in A. (D) Micrograph showing multiple blood vessels containing fibrin emboli (arrows). (E) Magnification of a vessel revealing the structure of a fibrin embolus.

Hematoxylin and eosin staining.

Magnifications:
A panoramic micrograph was obtained using an Aperio CS2-Digital Pathology Slide Scanner. B, 40x; C, 100x; D, 10x; E, 40x.

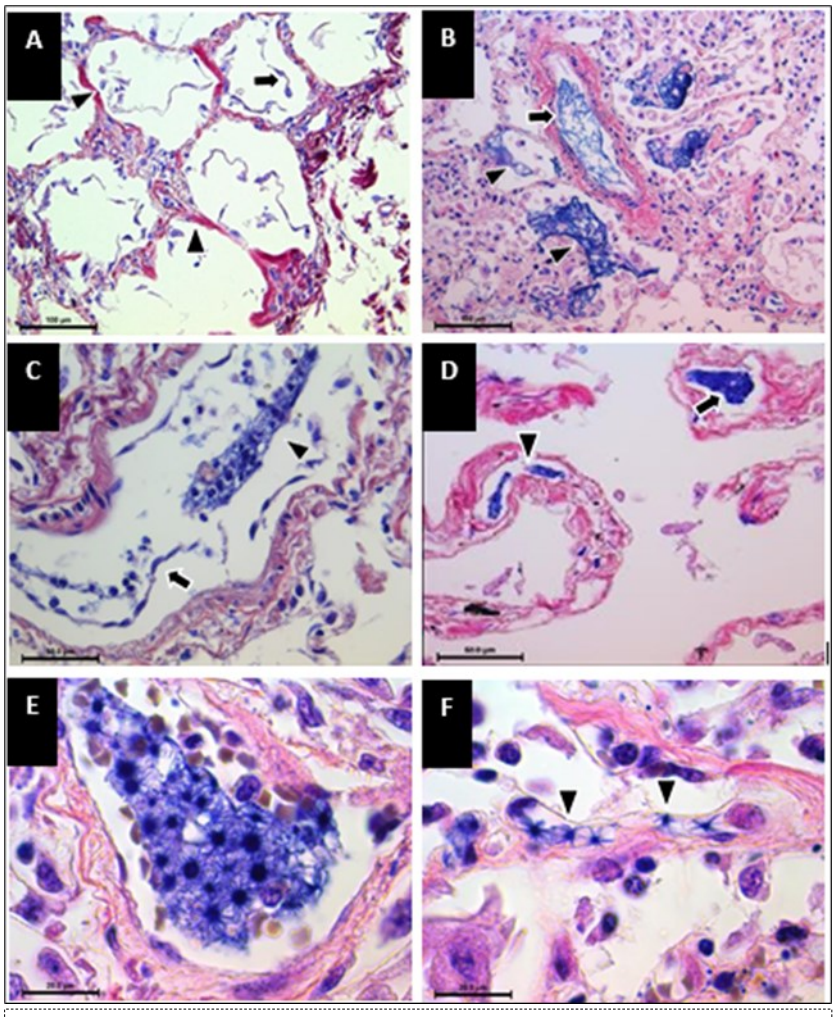

Figure 2. Fibrin thrombi in the lungs of patients who died of SARS-CoV-2 infection.

Tissue sections stained with phosphotungstic acid hematoxylin revealed diffuse alveolar damage (DAD) and thromboembolism in various anatomical locations.
(A) Hyaline membranes (arrowhead) and pneumocyte detachment (arrow).
(B) Thrombus in the arteriole (arrow) and intra-alveolar fibrin deposition (arrowheads).
(C) Endothelial cell detachment (arrow) and fibrin embolus (arrowhead) in the arterioles.
(D) Fibrin thrombi in the arterioles (arrow) and pulmonary capillaries (arrowhead).
(E) Star-shaped fibrin structure in the arterioles.
(F) Star-shaped fibrin structures in the pulmonary capillaries (arrowheads).

Phosphotungstic acid hematoxylin staining.

Magnifications:
(A, B) 20x; (C, D) 40x; (E, F) 100x.

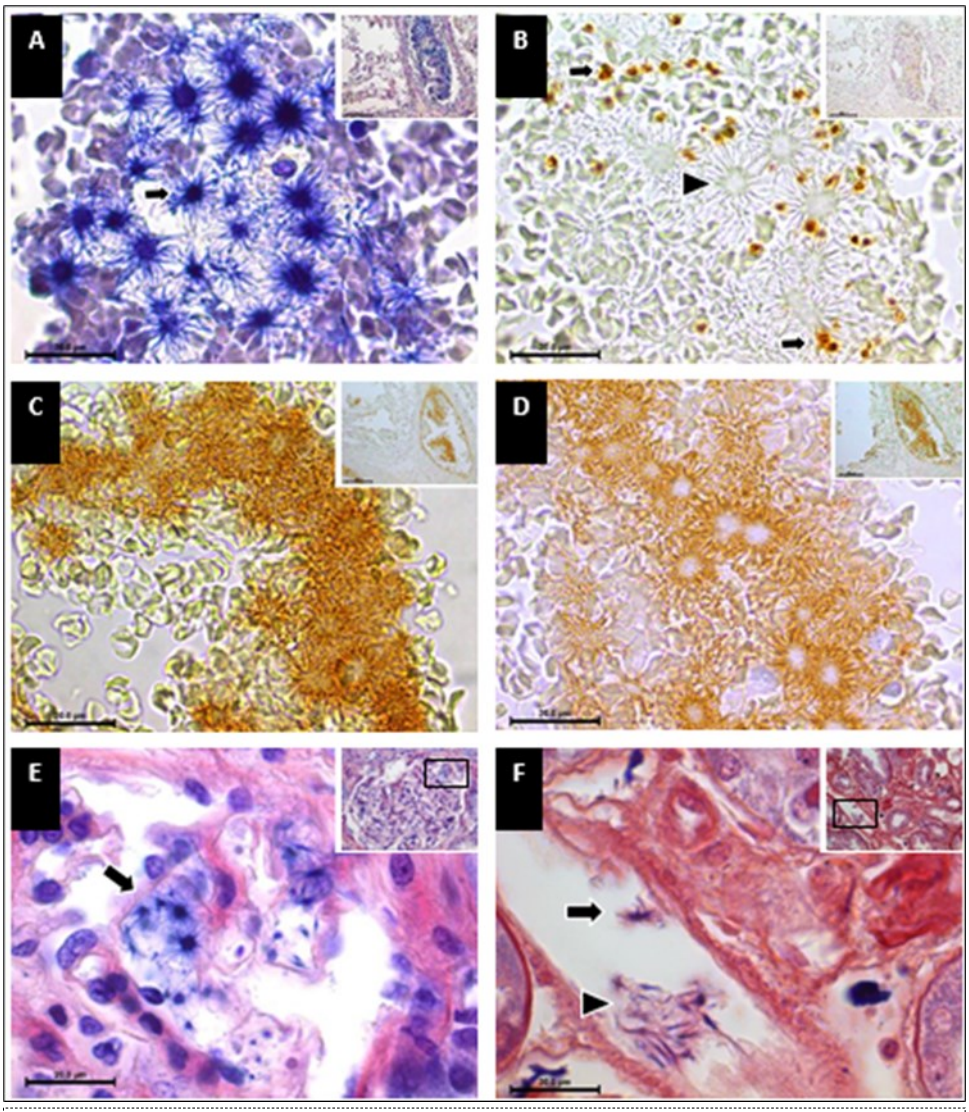

Figure 3. Star-shaped fibrin structures in pulmonary and renal microthrombi from deceased COVID-19 patients.

(A) PTAH-stained lung arteriole with star-shaped fibrin thrombus.

(B) CD61-positive platelet aggregates (arrows) in fibrin thrombus.

(C-D) Thrombus immunolocalization of VWF and factor VIII.

(E) Glomerular capillaries with star-shaped fibrin thrombi (arrows).

(F) Fibrin strands and star-shaped fibrin in a peritubular capillary.

Stains:

(A, E, F) PTAH stain; (B-D) Immunoperoxidase stain.

Magnifications:

(A-D) 100x, insets 20x; (E-F) 100x, insets 40x.

damage. Fibrin thrombi were identified in 12/16 (75%) analyzed cases. These thrombi were predominantly located in peritubular (10/12) and glomerular (8/12) capillaries. The fibrin structure observed in renal thrombi was mostly fibrillary. However, in 4/12 (33%) cases, star-shaped fibrin structures were found in the glomerular and peritubular capillaries (Fig. 3E-F). Collectively, thrombi with a star-shaped fibrin structure were observed in 7/40 autopsies (27.5%), with four cases located in

the lungs and four in the kidneys. Of these, only one patient had this fibrin conformation in both organs.

Morphometric Characteristics of the Star-shaped Fibrin Structures

The star-shaped fibrin structure is a conglomerate of discrete fibrin units, each consisting of a spheroid core, with fine fibrin needles radiating from it. The core had an irregular size with an average diameter of 4 µm. The overall size of the structure ranged from 12 to 15 µm. Thrombi with this fibrin pattern were observed more frequently in blood vessels located in areas of severe lung damage (1.04 ± 0.7 vessels/mm²) compared to areas of minimal damage (0.33 ± 0.3 vessels/mm²) ($p = 0.012$). In areas of minimal damage, this fibrin pattern was observed only in paraseptal pulmonary capillaries adjacent to areas of severe damage.

Discussion

SARS-CoV-2 infection has been associated with several health complications, including arterial and venous thromboembolism, inflammation, hypoxia, immobilization, and diffuse intravascular coagulation. Our histopathological findings align with those of other autopsy series of COVID-19 patients, showing DAD, microthrombi in pulmonary arterioles and capillaries, and fibrin deposition in the alveolar spaces. Tubular degenerative changes and glomerular damage in our kidney samples were also consistent with findings from other studies on deceased COVID-19 patients. Nevertheless, to the best of our knowledge, this study is the first to document the structural alterations in the fibrin network that may be associated with SARS-CoV-2 infection. The only prior study on this phenomenon was conducted by Juhlin and Shelley. In 1977, they reported the in vitro formation of fibrin asteroid bodies, which have an amorphous central region, likely composed of platelet aggregates surrounded by fine, radiating needle-like crystals. This was achieved by incubating blood samples from patients with psoriasis or vasculitis with bacterial extracts or gram-negative bacterial endotoxins. It is important to highlight three key differences between the structures observed by Juhlin and those observed in the present study.

First, Juhlin's observations were made *in vitro*, whereas our observations were made *in vivo*.

Second, PTAH staining revealed that the nuclei were composed of fibrin rather than platelets. This finding was confirmed through immunohistochemical analysis, as the nuclei showed no reaction to CD61, VWF, or Factor VIII (Fig. 3 A-D).

Third, the structures described by Juhlin range in size from 50 µm to 200 µm, whereas those described in this article range from 12 µm to 15 µm.

The results of Juhlin's study suggest that the structure of fibrin can be altered by bacterial products to adopt an asteroid shape. In light of these findings, we sought to investigate the potential correlation between bacterial co-infection and the formation of star-shaped fibrin structures in COVID-19 patients. Nevertheless, Fisher's exact test did not reveal a correlation between the fibrin pattern and the incidence of co-infection ($p = 0.397$).

An alternative approach to explain the formation of star-shaped fibrin bodies described in our study was to explore the potential relationship between coagulation and systemic inflammation parameters with the histopathological analysis. Although coagulation parameters were statistically similar in both groups, the analysis of systemic inflammation parameters CRP and NLR showed a tendency to be higher in the group with star-shaped fibrin bodies compared to those in the group with a reticular fibrin

pattern (Table 2). Although only the CRP levels reached statistical significance, this trend in inflammation parameters strongly supported the histopathological findings, which revealed the presence of star-shaped fibrin thrombi predominantly in vessels located in areas of lung tissue with marked inflammation. Therefore, it is possible to hypothesize that this pattern may be related to thrombi inflammation induced by the host's local immune response to SARS-CoV-2 infection.

Conclusion

This study reports the discovery of a star-shaped fibrin structural pattern present in pulmonary and renal thrombi of patients who died from COVID-19. However, further research is needed to investigate how these structures may contribute to disease severity and to elucidate the molecular mechanisms involved in their formation.

Abbreviations

COVID-19 - Coronavirus disease 2019; SARS-CoV-2 - Severe Acute Respiratory Syndrome Coronavirus 2; SARS - Severe Acute Respiratory Syndrome; ACE2 - Angiotensin-Converting Enzyme 2; RAAS - Renin-Angiotensin-Aldosterone System; ARDS - Acute Respiratory Distress Syndrome; DAD - Diffuse Alveolar Damage; RT-PCR - Real-Time Reverse Transcriptase-Polymerase Chain Reaction; INER - Instituto Nacional de Enfermedades Respiratorias; PTAH - Phospho-Tungstic Acid-Hematoxylin; PT - Prothrombin Time; aPTT - Activated Partial Thromboplastin Time; TT - Thrombin Time; D-D - D-Dimer; CRP - C-Reactive Protein; NLR - Neutrophil-to-Lymphocyte Ratio; VWF - von Willebrand Factor.

Statements

Statement of Ethics

The study protocol was reviewed and approved by the Research Ethics Committee of the National Institute of Respiratory Diseases, Ismael Cosio Villegas, Mexico City, Mexico (approval number - B05 -24). Written informed consent was obtained from each patient's relatives to perform autopsies.

Funding Sources

This study was not supported by any sponsors or funders.

Author Contributions

M, M-F., C, L-R., and JS, L-G - Conception, Design, and Formal Analysis. E, B-V - Performance of the microbiological test.

S, S-T, D, A-C, F, B-M - Acquisition and curation of data as well as execution of the research methodology.

All authors contributed to the initial draft and subsequent revisions, and approved the final version of the manuscript.

Data Availability Statement

All data generated or analyzed during this study are included in this article. Further inquiries can be directed to the corresponding authors.

Acknowledgement

The authors thank Javier Benjamín Contreras, Guadalupe Hiriart Valencia, and Erika Liliana

Monterubio Flores for their assistance with technical aspects of this study.

Conflict of Interest Statement

The authors have no conflicts of interest to declare.

References

1. Li W, Moore MJ, Vasilieva N, Sui J, Wong SK, et al. (2003). Angiotensin-converting enzyme 2 is a functional receptor for the SARS coronavirus. *Nature*, Nov 27; 426(6965):450-4. doi: 10.1038/nature02145.
2. Zhou P, Yang XL, Wang XG, Hu B, Zhang L, et al. (2020). A pneumonia outbreak associated with a new coronavirus of probable bat origin. *Nature*, Mar; 579(7798):270-273. doi: 10.1038/s41586-020-2012-7.
3. Ashraf UM, Abokor AA, Edwards JM, Waigi EW, Royfman RS, et al. (2021). SARS-CoV-2, ACE2 expression, and systemic organ invasion. *Physiol Genomics*, Feb 1; 53(2):51-60. doi: 10.1152/physiolgenomics.00087.2020.
4. Beyerstedt S, Casaro EB, Rangel ÉB. (2021). COVID-19: angiotensin-converting enzyme 2 (ACE2) expression and tissue susceptibility to SARS-CoV-2 infection. *Eur J Clin Microbiol Infect Dis*, May; 40(5):905-919. doi: 10.1007/s10096-020-04138-6.
5. Klavina PA, Leon G, Curtis AM, Preston RJS. (2022). Dysregulated haemostasis in thrombo-inflammatory disease. *Clin Sci (Lond)*, Dec 22; 136(24):1809-1829. doi: 10.1042/CS20220208.
6. Vasquez-Bonilla WO, Orozco R, Argueta V, Sierra M, Zambrano LI, et al. (2020). A review of the main histopathological findings in coronavirus disease 2019. *Hum Pathol*, 105:74-83. doi: 10.1016/j.humpath.2020.07.023.
7. Carsana L, Sonzogni A, Nasr A, Rossi RS, Pellegrinelli A, et al. (2020). Pulmonary post-mortem findings in a series of COVID-19 cases from northern Italy: a two-centre descriptive study. *Lancet Infect Dis*, Oct; 20(10):1135-1140. doi: 10.1016/S1473-3099(20)30434-5.
8. Elsoukkary SS, Mostyka M, Dillard A, Berman DR, Ma LX, et al. (2021). Autopsy Findings in 32 Patients with COVID-19: A Single-Institution Experience. *Pathobiology*, 88(1):56-68. doi: 10.1159/000511325.
9. Wichmann D, Sperhake JP, Lütgehetmann M, Steurer S, Edler C, et al. (2020). Autopsy Findings and Venous Thromboembolism in Patients With COVID-19: A Prospective Cohort Study. *Ann Intern Med*, Aug 18; 173(4):268-277. doi: 10.7326/M20-2003.
10. García-Ortega A, de la Rosa D, Oscullo G, Castillo-Villegas D, López-Reyes R, et al. (2021). Coagulation disorders and thromboembolic disease in COVID-19: review of current evidence in search of a better approach. *J Thorac Dis*, Feb; 13(2):1239-1255. doi: 10.21037/jtd-20-3062.
11. Fox SE, Akmatbekov A, Harbert JL, Li G, Quincy Brown J, et al. (2020). Pulmonary and cardiac pathology in African American patients with COVID-19: an autopsy series from New Orleans. *Lancet Respir Med*, Jul; 8(7):681-686. doi: 10.1016/S2213-2600(20)30243-5.
12. Dolhnikoff M, Duarte-Neto AN, de Almeida Monteiro RA, da Silva LFF, de Oliveira EP, et al. (2020). Pathological evidence of pulmonary thrombotic phenomena in severe COVID-19. *J*

Thromb Haemost, Jun; 18(6):1517-1519. doi: 10.1111/jth.14844.

13. Konopka KE, Wilson A, Myers JL. (2020). Postmortem Lung Findings in a Patient With Asthma and Coronavirus Disease 2019. *Chest*, Sep; 158(3) . doi: 10.1016/j.chest.2020.04.032.
14. Tian S, Hu W, Niu L, Liu H, Xu H, et al. (2020). Pulmonary Pathology of Early-Phase 2019 Novel Coronavirus (COVID-19) Pneumonia in Two Patients With Lung Cancer. *J Thorac Oncol*, May; 15(5):700-704. doi: 10.1016/j.jtho.2020.02.010.
15. Su H, Yang M, Wan C, Yi LX, Tang F, et al. (2020). Renal histopathological analysis of 26 post-mortem findings of patients with COVID-19 in China. *Kidney Int*, 98(1):219-227. doi: 10.1016/j.kint.2020.04.003.
16. Rossi GM, Delsante M, Pilato FP, Gnetti L, Gabrielli L, et al. (2020). Kidney Biopsy Findings in a Critically Ill COVID-19 Patient With Dialysis-Dependent Acute Kidney Injury: A Case Against "SARS-CoV-2 Nephropathy". *Kidney Int Rep*, May 17; 5(7):1100-1105. doi: 10.1016/j.ekir.2020.05.005.
17. Juhlin L, Shelley WB. (1977). Oriented fibrin crystallization: A phenomenon of hypersensitivity to bacteria in psoriasis, vasculitis and other dermatoses. *Br J Dermatol*, Jun; 96(6):577-86. doi: 10.1111/j.1365-2133.1977.tb05200.x.
18. Lin J, Yan H, Chen H, He C, Lin C, et al. (2021). COVID-19 and coagulation dysfunction in adults: A systematic review and meta-analysis. *J Med Virol*, Feb; 93(2):934-944. doi: 10.1002/jmv.26346. Epub 2020 Aug 2. PMID: 32706426; PMCID: PMC7405098.